THE JOURNAL OF PHYSICAL CHEMISTRY B

Article

Cite This: J. Phys. Chem. B 2018, 122, 4566−4572

pubs.acs.org/JPCB

Diffusivity of Carbon Dioxide in Aqueous Solutions under Geologic Carbon Sequestration Conditions

Pradeep N. Perera,*[,†] Hang Deng,[†] P. James Schuck,[‡] and Benjamin Gilbert[†]

[†]Energy Geosciences Division, Lawrence Berkeley National Laboratory, Berkeley, California 94720, United States

[‡]Molecular Foundry, Lawrence Berkeley National Laboratory, Berkeley, California 94720, United States

ABSTRACT: Accurate assessment of the long-term security of geologic carbon sequestration requires knowledge of the mobility of carbon dioxide in brines under pressure and temperature conditions that prevail in subsurface aquifers. Here, we report Raman spectroscopic measurements of the rate of CO_2 diffusion in water and brines as a function of pressure, salinity, and concentration of CO_2. In pure water at 50 ± 2 °C and 90 ± 2 bar, we find the diffusion coefficient, D, to be (3.08 ± 0.03) × 10^{-9} m^2/s, a value that is consistent with a recent microfluidic study but lower than earlier PVT measurements. Under reservoir conditions, salinity affects the mobility of CO_2 significantly and D decreased by 45% for a 4 M solution of NaCl. We find significant differences of diffusivity of CO_2 in brines (0−4 M NaCl), in both the absolute values and the trend compared to the Stokes−Einstein prediction under our experimental conditions. We observe that D decreases significantly at the high CO_2 concentrations expected in subsurface aquifers (∼15% reduction at 0.55 mol/kg of CO_2) and provides an empirical correction to the commonly reported D values that assume a tracer concentration dependence on diffusivity.

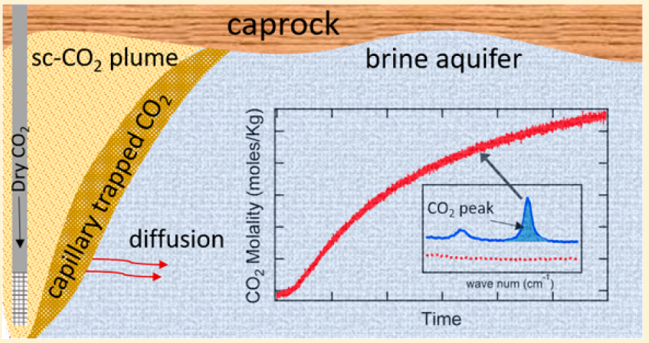

INTRODUCTION

The removal of anthropogenic carbon dioxide (CO_2) by geologic carbon sequestration (GCS) is expected to be an important approach to mitigating CO_2 emission to the atmosphere from hydrocarbon combustion while transitioning to a clean-energy economy.[1,2] In the GCS concept, supercritical CO_2 ($scCO_2$) is injected into aquifers at depths of 1−3 km where capillary trapping in pores, dissolution into brine, and precipitation as carbonate minerals enable long-term carbon sequestration. Following injection and pressure- and buoyancy-driven advection, CO_2 diffusion into the formation is a necessary transport process for mineral sequestration reactions; hence, knowledge of the diffusivity of CO_2 under GCS conditions is important for all modeling assessments of the feasibility of the secure entrapment of CO_2.

Several approaches have been developed for the quantitation of diffusion coefficient D of CO_2 in an aqueous solution.[3,4] Traditionally, the pressure−temperature−volume (PVT) technique,[5] based on the pressure drop of the gas phase, provides a macroscopic measurement of the diffusivity of CO_2 in water under reservoir-like conditions. Despite the simplicity, it has been shown that PVT methods lack the ability to capture microscopic details of the process and are prone to error due to, for example, density-driven mixing in the system. Taylor dispersion[6] has also been frequently used for diffusivity measurement and has been successfully used to measure the diffusivity of CO_2 in pure water at elevated temperature and pressure.[7] Recently, alternative optical spectroscopic methods have been used to determine the diffusivity of CO_2 in aqueous solutions. For example, Lu et al. used Raman spectroscopy to determine D of CO_2 in pure water in wide ranges of temperature (−5−200 °C) and pressure (100−450 bar).[8]

While the diffusivity of CO_2 in pure water has been studied extensively, under both ambient conditions and at high pressure and temperature, GCS conditions are characterized by high concentrations of brines as well as high concentrations of CO_2, yet the effects of salinity and diffusing tracer concentration (CO_2) on D have not been studied thoroughly. Indeed, recent reports of the absolute value of the diffusion coefficient, D, in saline solutions and its dependence on salinity show significant variations. For example, a study that used a pH-sensitive dye and fluorescence spectroscopy to monitor the CO_2 transport in brines found that diffusivity drops nearly 50% between 0 and 4 M NaCl concentrations at 26 °C and 5 bar.[9] At the same temperature, a pulsed field gradient (PFG)-NMR study reported a drop of, based on extrapolations of their data, 30% in diffusivity over the same salinity range.[7] A Raman spectroscopy study at 21 °C found a drop of ∼30% under similar salinity conditions.[10] Both linear[7,9] and nonlinear[10] dependences of D on salinity have been reported. However, the salinity effect under reservoir-like conditions has not been reported to date.

Received: January 23, 2018
Revised: March 27, 2018
Published: March 27, 2018

DOI: 10.1021/acs.jpcb.8b00802
J. Phys. Chem. B 2018, 122, 4566−4572

Moreover, the assumption that infinite-dilution CO_2 diffusivity will accurately predict the diffusivity of CO_2 in GCS reservoirs[3,4] has never been experimentally tested.

To clarify the diffusion behavior of CO_2 under realistic reservoir conditions, and to pursue a research program on fluid and mineral reactions relevant to GCS, we have constructed a Raman microscope that is compatible with high-pressure, high-temperature capillaries and microfluidic cells that operates routinely up to 100 bar and 80°C with imaging capabilities at diffraction-limited spatial resolution (i.e., ∼300 nm). In this article, we report the measurements of the diffusion kinetics of CO_2 in pure water and brines (0−4 M NaCl) up to supercritical conditions (60−100 bar at 50 °C). These results provide new observations. First, we report the effect of salinity on diffusivity under GCS conditions. The diffusivity of CO_2 drops as much as 45% at 4 M NaCl concentration from its value in pure water and shows that the dependence of D on salinity is not fully described by the standard Stokes−Einstein relationship. Second, we quantify the influence of CO_2 concentration on the net diffusion of this species. On the basis of numerical simulations, we report that the diffusivity of CO_2 drops ∼15% at 0.55 mol/kg of CO_2 and can be modeled by the second-order dependence on concentration under the reservoir-like conditions presented here.

EXPERIMENT

Millipore water (18.1 Ω) was used for all experiments. NaCl(s) (Sigma-Aldrich; 99.9% purity) and CO_2(g) (Praxair; 99.999% purity) were used as received.

Fluidic System. Figure 1A shows a simplified diagram of the experimental setup that was designed to generate concentration profiles of CO_2 in water (or in brines) as a function of time at 90 ± 2 bar and 50 ± 2 °C. The fluid handling system consists of two Teledyne ISCO model 100DM pumps (pumps A and B), two Chemyx Nexus 6000 pumps (pumps C and D), and stainless steel and PEEK tubing and valves to deliver and control the flow pattern at high pressure and temperature. A homemade right-angle PEEK holder (Figure 1B) connects fused silica capillaries (Polymicro Technologies; 150 or 200 μm diameter) to the fluidic system. The entire fluidic setup, with the exception of the pumps, is kept in an insulated box in which the temperature was controlled with an active PID controller (Omega Engineering, model CN8DPt)) within ±2 °C. In a typical experiment, the fluidic pathway is thoroughly flushed (to remove air in the system) and filled with water (or brines) among valves V_1, V_2, and V_3 with pump A. Thereafter, with valve V_2 closed, pumps B and C are synchronized in a "push−pull" motion to deliver and withdraw $scCO_2$ to and from the system. This process replaces water (or brine) between V_1 and V_3 with $scCO_2$ (the flow path indicated in yellow in Figure 1B) while leaving a trapped stationary water/brine column in the capillary tubing from point A to V_2 (blue line). This procedure establishes a stable aqueous/$scCO_2$ interface at point A (x = 0) in the PEEK adapter.

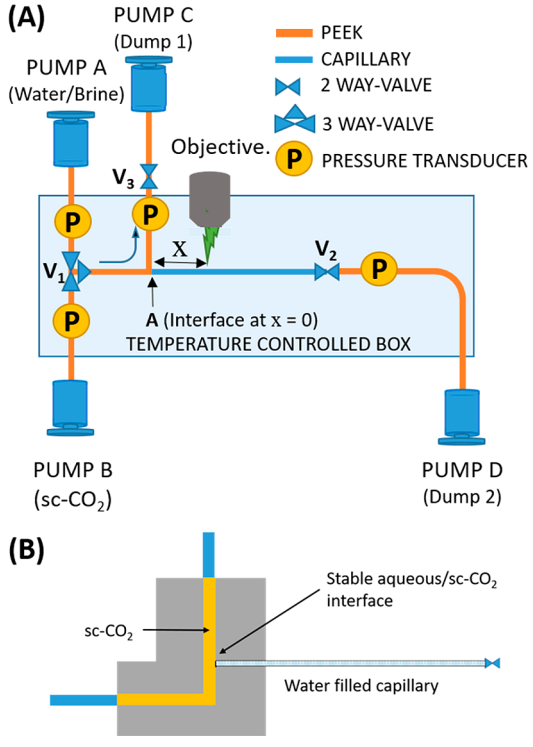

Figure 1. (A) Schematic diagram of the experimental setup used for the diffusion experiment. (B) PEEK holder that connects the capillary tubing to the fluidic system.

Raman Microscope. A home-built Raman microscope was used for this research. The microscope is a Nikon Eclipse Ti-U with a 20x Nikon objective with a 7.6 mm working distance. Raman spectra are acquired by using a 532 nm laser (Spectra-Physics EXLSR-532-300-CDRH), a Princeton Instruments Acton Spectropro SP-2358 spectrometer (300 mm focal length, 600 lines/mm, and 750 nm blazed grating), and a back-illuminated PIXIS 100 Br charge-coupled device (CCD). The Nikon objective was partially immersed in a temperature-controlled enclosure with air-circulating fans to minimize thermal drifts and gradients.

Raman Data Collection and Analysis. Each diffusion experiment was started by creating a fresh interface between $scCO_2$ and water (or brines) at a given pressure and temperature at point A (x = 0) as shown in Figure 1B. Microscopic observations of the $scCO_2$−water interface confirmed that it was stable and static. The objective was focused on the center of the capillary tube at a distance x (7.75−13.75 mm) from the interface. Raman spectra were integrated for 10 s to achieve a good signal-to-noise ratio, resulting in a time series of CO_2 concentrations over 6000−30 000 s, a time scale that is much larger than breakthrough time. The concentration of CO_2(aq) at distance x was quantified as a function of time using the integrated intensity of the Raman signal from CO_2 in the 1325−1430 cm^{-1} region, one of the Fermi dyad peaks that results from the coupling of symmetric stretching mode ν_1 and the first overtone of bending mode ν_2.[11] All spectra were normalized to the Raman peak of water (2800−3600 cm^{-1}) as described below.

First, the baseline contribution to the Raman peak of water (2800−3600 cm^{-1}) and CO_2 (1325−1430 cm^{-1}) was removed by fitting the baseline to a first-order polynomial. After baseline subtraction, the intensity under the Raman peaks was integrated for CO_2 (α_{CO_2}) and pure water (α_{H_2O}) [or brines (α_{brine})]. The integrated intensity under the CO_2 peak was normalized to that of pure water ($\alpha_{CO_2}/\alpha_{H_2O}$) or to that of brine ($\alpha_{CO_2}/\alpha_{brine}$) to remove instrumental variations such as changes in laser intensity or the focal point from run to run.

The normalized Raman cross section of CO_2 (Ω) is calculated by using the normalized integrated intensity under the CO_2 peak of a saturated CO_2 solution at 50 ± 2 °C and

DOI: 10.1021/acs.jpcb.8b00802
J. Phys. Chem. B 2018, 122, 4566−4572

90 ± 2 bar, which has a known solubility of 1.08 mol/kg,[12] according to eq 1.

$$\Omega = (\alpha_{CO_2}/\alpha_{H_2O})_{sat}/1.08 \quad (1)$$

The concentration of CO_2 at a given time was calculated by dividing the normalized integrated intensity under the CO_2 peak ($\alpha_{CO_2}/\alpha_{H_2O}$) by a Raman cross section of CO_2 (Ω) determined by eq 1. A similar approach was taken to determine the concentration of CO_2 in brines.

Convection and advection processes, such as density-driven mixing and natural (buoyancy) convection, can interfere with the measurements of diffusion coefficients. We minimized density-driven mixing by holding the capillary system horizontally. The entire set up was kept in a constant-temperature enclosure, thus avoiding temperature gradients across the capillary tubes. The swelling of the brine phase upon CO_2 diffusion has been observed at high pressures.[13] However, the stationary aqueous/scCO_2 interfaces observed in our experiments implicate that no significant swelling of the aqueous phase has occurred under our experimental conditions.

Analytical Fits to Diffusion Data. Assuming that the diffusion coefficient (D) is independent of concentration, Fick's second law (eq 2)[14] can be solved for a one-dimensional system analytically.

$$\frac{\partial c}{\partial t} = D\frac{\partial^2 c}{\partial x^2} \quad (2)$$

The solution shows that concentration at time t at distance x from the interface is given by eq 3 for a semi-infinite cylindrical geometry (i.e., length ≫ radius).

$$C(t, x) = C_{sat}\mathrm{erfc}\left(\frac{x}{(4Dt)^{1/2}}\right) \quad (3)$$

for the boundary conditions: (1) $C(t) = 0$ at $t = 0$, $x > 0$ and (2) $C(t) = C(0)$ at $x = 0$, $t = 0$. C_{sat} is the concentration of the solute at saturation. We used models developed by Duan et al.[12] to calculate this quantity. We fitted eq 3 to experimental CO_2 concentration profiles using a nonlinear least-squares optimization tool provided in Matlab (R2010b). To accommodate any subtle changes in distance, x was used in the equation as a fitting parameter with tight (±3%) boundary controls on the measured values.

Numerical Simulations of Diffusion. In order to test the applicability of Fick's second law under GCS conditions, we investigated the validity of the assumption that the diffusion coefficient is independent of CO_2 concentration. To this end, we performed numerical simulations using CrunchFlow,[15] a multicomponent reactive transport code. Numerical simulation was set up as follows. It is assumed that at the scCO_2/water interface, the water phase equilibrates with scCO_2 instantaneously, reaching a saturated concentration, C_{sat}. This imposes a Dirichlet constant-concentration boundary condition on the aqueous side of the interface. C_{sat} is taken to be a function of the experimental pressure and temperature.[12] A one-dimensional computational domain was used to represent the capillary tube. The discretization was refined such that further refinement of the mesh did not affect the simulations results statistically. For the simulations without the consideration of the concentration dependence of the diffusion coefficient, discretization of the diffusion-reaction equation is given as follows

$$\frac{C_i^{t+\Delta t} - C_i^t}{\Delta t} = D\frac{(C_{i+1}^t + C_{i-1}^t - 2C_i^t)}{\Delta x^2} + R(C_i^t) \quad (4)$$

For the simulations with the consideration of the concentration dependence of the diffusion coefficient, diffusion coefficient $D(C_i)$ is a function of the concentration of CO_2 and varies with space. The discretized diffusion-reaction equation is instead given as the following equation

$$\frac{C_i^{t+\Delta t} - C_i^t}{\Delta t} = \frac{D(C_i)\frac{(C_{i+1}^t - C_i^t)}{\Delta x} - D(C_{i-1})\frac{(C_i^t - C_{i-1}^t)}{\Delta x}}{\Delta x} + R(C_i^t) \quad (5)$$

Dissociation of the carbonate species was also included in the numerical simulations.

RESULTS AND DISCUSSION

***D* in Pure Water.** The ability of Raman spectroscopy to detect CO_2 in aqueous media provides a direct and simple way to quantify CO_2 in solution over other optical methods. Typical Raman spectra acquired at the beginning of and during a diffusion experiment are shown in Figure 2A. Initially, only the Raman peak of water is detectable, and as the diffusion progresses, characteristic Raman signatures of CO_2(aq) appear in

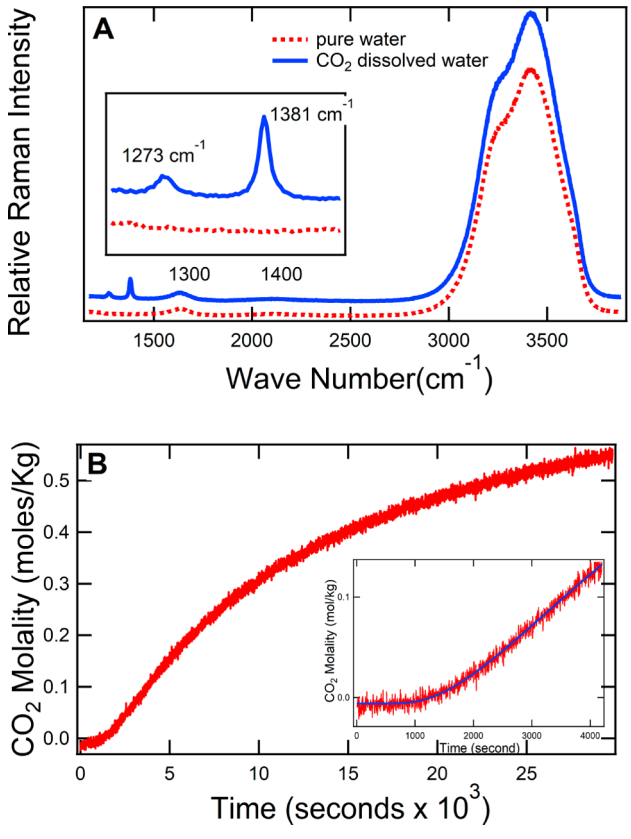

Figure 2. Quantification of CO_2 concentration and diffusion rate in high-pressure aqueous solutions using Raman spectroscopy. (A) Raman spectra at $t = 0$ (pure water; red ---) and at $t = 4000$ s (CO_2 dissolved water; blue —). (A Inset) Spectral region 1200−1500 cm^{-1} showing the Fermi dyad, resulting from the coupling of symmetric stretching mode ν_1 and first overtone of bending mode $2\nu_2$ of CO_2(aq). Spectra were offset for clarity. (B) Diffusion profile of CO_2 in a pure-water-filled 200 μm capillary measured 7.75 mm away from the interface. The profile was obtained by integrating the area 1325−1430 cm^{-1} and normalizing it to the area of the water peak. (B Inset) Nonlinear least-squares fit of the analytical solution of Fick's second law (eq 2; blue line) to the experimental data (red line). The fit is calculated only to the duration of the experiment for which the CO_2 concentration remained below 0.07 mol/kg.

DOI: 10.1021/acs.jpcb.8b00802
J. Phys. Chem. B 2018, 122, 4566−4572

the Raman spectrum at 1273 and 1381 cm^{-1} (Figure 2A inset). The concentration profiles of CO_2 obtained by integrating the area under the Raman peak between 1325 and 1430 cm^{-1}, as detailed in the experiment section, are shown in Figure 2B. In order to obtain D, the diffusion coefficient of CO_2, we fitted experimental concentration profile data to eq 3. As discussed later in the article, deviations from Fick's second law were observed at higher dissolved CO_2 concentrations under GCS conditions. Therefore, we first limited the analysis to CO_2 concentrations below 0.07 mol/kg to obtain the diffusion coefficient with eq 3 (Figure 2B inset). The D value that is determined from fitting the low-concentration data will be referred to as measured D for the experiments performed under different P, T and salinity conditions.

We verified that our measurements of D were independent of the specific choice of the experimental parameters by measuring the diffusion in two different capillary inner diameters (ID), either 150 or 200 μm, and at three different distances from the CO_2/water interface to the Raman measurement position (x), which ranged from 7.75 to 13.75 mm. Measured D values are shown in Figure 3. Under these conditions, at 50 ± 2 °C and

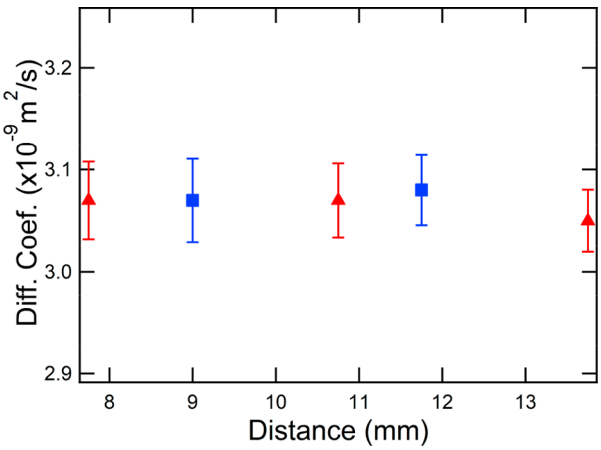

Figure 3. Measured diffusion coefficient (D) of CO_2 in pure water at 90 ± 2 bar and 50 ± 2 °C obtained from measurements at different distances (x = 7.75–13.75 mm) from the CO_2/water interface ina 200 μm diameter capillary (red ▲) and in a 150 μm diameter capillary (blue ■). Error bars are the standard deviation of at least three measurements. The average for all measurements is D = (3.08 ± 0.03) × 10^{-9} m^2/s.

90 ± 2 bar, we estimate D of CO_2 in pure water to be (3.08 ± 0.03) × 10^{-9} m^2/s. Our observation is at the lower end of the previously reported measurements at 50 ± 2 °C in pure water. For example, at 50 °C, Thomas and Adams reported D to be (3.35 ± 0.03) × 10^{-9} m^2/s at 1 bar in a free-flowing jet,[16] and more recent Raman spectroscopic work of Lu et al. reported D to be (3.21 ± 0.03) × 10^{-9} m^2/s in a capillary with a larger i.d. (300 μm).[8] Our result may be more reliable than the preceding studies because of the care taken here to avoid convection, which may artificially increase mixing and dispersion, and therefore will result in larger values of measured D. Cadogan et al., with the use of pulse-gradient NMR, reported a higher D of (3.64 ± 0.05) × 10^{-9} m^2/s.[7] As discussed in more detailed later, we find several points of discrepancy between our work and the pulse-gradient NMR data. We further confirmed the accuracy of our experimental approach by measuring D in pure water at 25 °C and found identical values to those reported by Sell et al.,[9] who also used a narrow-i.d. microfluidic cell with fluorescence microscopy.

Pressure Dependence of *D*. Recent experimental work below the supercritical conditions and moderate pressures (26 °C and between 5 and 50 bar)[9] and above critical-point pressures (140–493 bar)[7] have demonstrated that pressure makes a minimal contribution to diffusivity. Here, we report measurements at 50 ± 2 °C for the pressure range of 60–103 bar, which bridges the transition between the gaseous and supercritical states of CO_2, finding that D is independent of the pressure within the margin of error (Figure 4). Our results show that

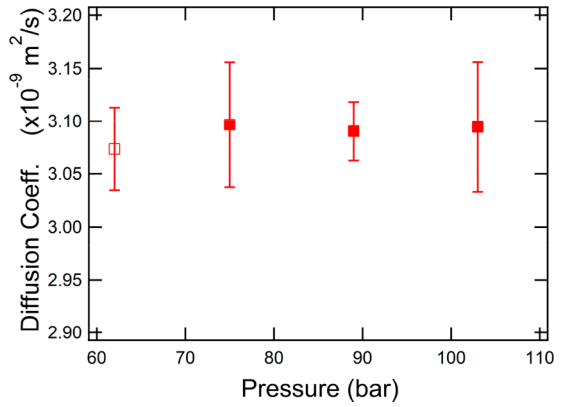

Figure 4. Measured diffusion coefficient (D) of CO_2 in water for the pressure range of 60–103 bar at 50 ± 2 °C. D is independent of the pressure range that bridges the gaseous and supercritical phases of CO_2. Open square denotes the CO_2 in the gaseous state while solid squares represent the supercritical phase.

pressure does not change the diffusivity of CO_2 in water; furthermore, the change in the phase of CO_2 does not, as expected, alter the diffusivity in solution.

Salinity Dependence of *D*. One of the main goals of this work is to determine the effect of salinity on the diffusivity of CO_2 under reservoir-like conditions. Salinity in GCS formations can reach 100 g salt/kg water, predominantly as sodium chloride, which lowers the rate of solute diffusion. By analogy to particle hydrodynamics, the decrease in the diffusion coefficient with salinity is often modeled as an effect of the altered viscosity of solution η and predicted by the Stokes–Einstein relationship

$$D = k_B T / n_{SE} \pi \eta a \quad (6)$$

where k_B is Boltzmann's constant, T is the absolute temperature, a is the solute hydrodynamic radius, and n_{SE} is the Stokes–Einstein number.

Our observations of the effect of salinity on the diffusivity of CO_2 are shown in Figure 5. Between 0 and 4 M NaCl concentrations at 90 ± 2 bar and 50 ± 2 °C, we observe that D decreases by 45 ± 2%. As mentioned earlier, there are no reports on CO_2 diffusivity in brines under GCS conditions for a direct comparison with our results. To compare with available data under different conditions, our observation of a decrease in D due to salinity has shown a similar magnitude (i.e., ~50%) within the margin of error of the fluorescence microspectroscopic data acquired at 26 °C in a microfluidic cell[9] but significantly higher than the reported values for PFG-NMR[7] (30% decrease at 25 °C) and Raman (30% decrease at 21 °C)[10] for the same salinity range. The later Raman study finds the diffusivity to be linearly correlated with salinity while our results[9] are best described by an exponential decay. Since there are no experimental reports available to compare directly with our

DOI: 10.1021/acs.jpcb.8b00802
J. Phys. Chem. B 2018, 122, 4566–4572

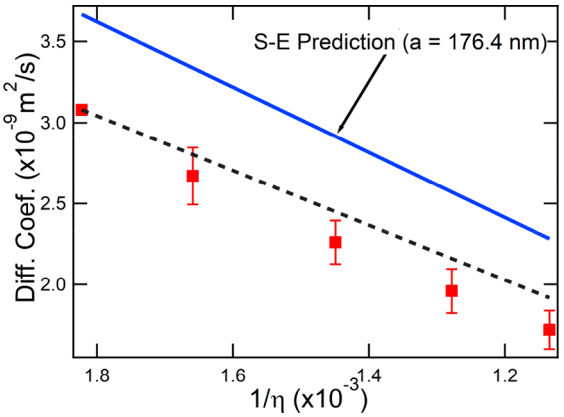

Figure 5. Dependence of the diffusion coefficient (D) of CO_2 on the viscosity of the solution, $1/\eta$, in 0–4 M solutions of NaCl at 50 ± 2 °C and 90 ± 2 bar. The solid blue line is the Stokes–Einstein prediction that used a hydrodynamic radius, a = 176.4 pm. The dashed black line is the SE prediction for a = 210 nm that was made based on our experimental D for CO_2 in pure water (the leftmost data point) at 50° ± 2C and 90 ± 2 bar. (See text for details.)

measurements of the absolute value of D, we have used the methodology adopted by Cadogan et al. to find the Stokes–Einstein estimate relevant to our conditions (50 ± 2 °C and 90 ± 2 bar). In two papers, Cadogan et al.[7] first showed that the Stokes–Einstein (SE) equation (eq 6) with a modification to the hydrodynamic radius of carbon dioxide, $a_{T(K)}$, to account for temperature could describe the D between 25 and 150 °C in pure water. Subsequently, they reported[7] that the SE relationship, with $a_{T(K)}$ at 298 K determined in pure water, correctly predicted the D in brines at the same temperature in the range of 0–5 M NaCl, essentially declaring the hydrodynamic radius of CO_2 to be independent of the salinity in the system. Using the relationship, $a_T = a_{298}[1 + \alpha(T(K) - 298)]$, given by Cadogan et al.,[7] where $\alpha = 2.0 \times 10^{-3}$ and a_{298} = 168 pm, we determined a_{323} to be 176.4 pm for our conditions. Thereafter, with a_{323} and viscosity data from the literature,[17] we calculated the SE prediction of the salinity dependence of CO_2 diffusivity in brine at 50 ± 2 °C and 90 ± 2 bar. As shown in Figure 5, SE predictions are greater than the measured values by 20–30% from 0–4 M NaCl. Cadogan et al.[7] noted significant disagreement with the fluorescence microspectroscopic data[9] at 26 °C with this approach. More interestingly, we find that the single hydrodynamic radius of CO_2 cannot represent experimental D values with increasing salinity. For example, as shown in Figure 5 (dashed black line), the SE prediction with a_T = 210 nm, arbitrarily selected to match our experimental D of CO_2 in pure water (leftmost data point), would deviate from the experimental D in brine as the salinity increases from 0 to 4 M. This observation suggests of a molecular level change in the hydration shell structure of CO_2 with increasing salinity.

It is not surprising that the Stokes–Einstein approach, developed to deal with the diffusivity of hard, smooth spheres, yields predictions that deviate from experimental results for the diffusivity of a small molecule in a strongly hydrogen-bonded medium. Numerous modifications have been proposed to relax the hard sphere assumption, to consider when the size of the tracer molecule approaches that of the solvent,[18] and to better account for the viscosity[19] and temperature[20] dependence. Furthermore, theoretical studies have shown the relevance of the microscopic details that are neglected in the macroscopic SE view.[21,22] It was unexpected, however, to find agreement of PFG-NMR with the SE prediction that disagrees with other optical methods in the absolute values of D (for fluorescence measurements performed at 25 °C)[9] and in the trend in D with viscosity (albeit at different temperatures) for data determined by the present macroscopic diffusion study.

The PFG-NMR method is a well-established approach for obtaining molecular diffusion coefficient measurements.[23,24] We propose that the discrepancy could be due to the chemical reactivity of dissolved CO_2 with water as shown in eq 7. Bicarbonate dissociation has a negligible presence under our experimental (pH) conditions and therefore was omitted from consideration.

Although under our experimental conditions the majority of CO_2 is present as the solvated CO_2, this pool is in dynamic equilibrium with a fraction (~1/650) in the form of carbonic acid. The hydration rate of CO_2(aq), $k_1 + k_2 = 0.040 \pm 0.003$ S^{-1},[25] which is on a time scale that is slower than the PFG-NMR measurement time, could lead to a net reduction in the macroscopic diffusion rate that is not detectable by the PFG method.

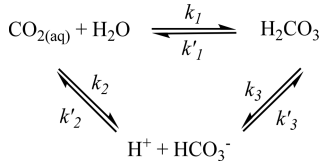

(07)

Further studies on the molecular interactions among CO_2, water and electrolyte ions, and kinetic models that combine translation and reaction would be required to test this suggestion.

Concentration Dependence of *D*. As discussed above, the analytical solution to Fick's second law shown in eq 3 uses the assumption that D is independent of concentration. This assumption is accurate for the low concentrations of dissolved CO_2 found in water or brine under ambient conditions and has been justified for high pressures due to the negligible changes in density and viscosity of the aqueous phase but has not been tested experimentally for the elevated CO_2 concentrations that are encountered at high pressures under GCS conditions. In Figure 6, we compare the experimental concentration profile of CO_2 in pure water at 90 ± 2 bar and 50 ± 2 °C with the

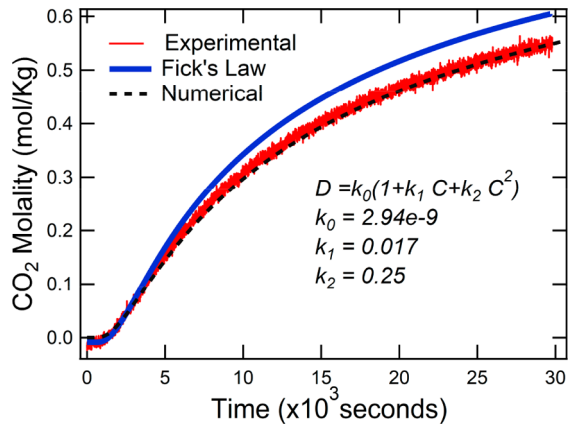

Figure 6. Dependence of diffusion coefficient D on CO_2 concentration. The experimental concentration of CO_2 as a function of time (red solid line) is poorly described at higher concentrations of CO_2 by the analytical solution eq 3 to the Fick's second law (blue solid line). The numerical prediction of CO_2 concentration with a second-order concentration correction to D, eq 8, provides significantly better agreement (black dashed line).

DOI: 10.1021/acs.jpcb.8b00802
J. Phys. Chem. B 2018, 122, 4566–4572

predicted concentration profile that assumes D to be independent of CO_2 concentration. The latter determination was made by first applying eq 3 to the experimental concentration profile below 0.07 mol/kg of CO_2 to determine Fick's diffusion coefficient D and subsequently reapplying D to eq 3 to determine the concentration of CO_2 ($C(t, x)$) for the entire concentration range. The analytical solution overpredicts the CO_2 concentration and therefore the diffusivity at higher concentrations, thus demonstrating the influence of the CO_2 concentration on D. To account for the discrepancy, we have used reactive transport modeling to calculate the diffusion coefficient as a function of concentration. By writing D as a second-order polynomial of concentration

$$D = k_0(1 + k_1C + k_2C^2) \quad (8)$$

where k_0, k_1, and k_2 are constants, we were able to reproduce the experimental concentration profile of CO_2 in pure water ($k_0 = 2.94e^{-9}$, $k_1 = 0.017$, and $k_2 = 0.25$ at 90 bar and 50 °C for pure water). As shown by the dashed line in Figure 6, this correction provides good agreement between the experimental data and the numerical calculation of the CO_2 concentration in the aqueous phase. The analysis shows that D drops by up to 15% at 0.55 mol/kg of CO_2 under these conditions in pure water. The second-order dependence of D on the concentration of CO_2 (eq 8) is applicable to only the above conditions and has not been tested for other temperature and pressure conditions and salinity.

CONCLUSIONS

Direct Raman spectroscopy observation and quantification of CO_2 in aqueous fluids under GCS conditions provide an accurate approach to measuring the CO_2 diffusivity. In addition to contributing new measurements for D, the results highlight the need to better understand the molecular processes that govern diffusion-based mass transportation. The faster reduction in D with increasing salt concentration compared to that predicted by the Stokes−Einstein, the dependence of the hydrodynamic radius of the solute on salinity, and the decline in D with increasing CO_2 concentration must consider microscopic solute−solvent (CO_2 and water) and solute−solute (CO, Na^+, and Cl^-) interactions for an explanation and are not yet fully described by molecular simulations or theories for solution thermodynamics.

AUTHOR INFORMATION

Corresponding Author

*E-mail: pperera@lbl.gov.

ORCID

Pradeep N. Perera: 0000-0002-0449-199X

Hang Deng: 0000-0001-5784-996X

Benjamin Gilbert: 0000-0003-0853-0826

Notes

The authors declare no competing financial interest.

ACKNOWLEDGMENTS

This work was supported by the Center for Nanoscale Controls on Geologic CO_2 (NCGC), an Energy Frontier Research Center funded by the U.S. Department of Energy, Office of Science, Basic Energy Sciences under award no. DE-AC02-05CH11231. The Raman measurements were performed at the Molecular Foundry, a national user facility supported by the Office of Science, Office of Basic Energy Sciences, of the U.S. Department of Energy under contract no. DE-AC02-05CH11231. We thank Ed Wong for design and engineering support and Youngman Kim and Jiamin Wan for advice on high-pressure fluidics.

REFERENCES

(1) DePaolo, D. J.; Cole, D. R. In *Geochemistry of Geologic CO_2 Sequestration*; DePaolo, D. J., Cole, D. R., Navrotsky, A., Bourg, I. C., Eds.; Mineralogical Soc Amer: Chantilly, VA, 2013; Vol. 77, pp 1−14.

(2) Song, J.; Zhang, D. X. Comprehensive Review of Caprock-Sealing Mechanisms for Geologic Carbon Sequestration. *Environ. Sci. Technol.* **2013**, *47*, 9−22.

(3) Garcia-Rates, M.; de Hemptinne, J. C.; Avalos, J. B.; Nieto-Draghi, C. Molecular Modeling of Diffusion Coefficient and Ionic Conductivity of CO2 in Aqueous Ionic Solutions. *J. Phys. Chem. B* **2012**, *116*, 2787−2800.

(4) Mutoru, J. W.; Leahy-Dios, A.; Firoozabadi, A. Modeling Infinite Dilution and Fickian Diffusion Coefficients of Carbon Dioxide in Water. *AIChE J.* **2011**, *57*, 1617−1627.

(5) Riazi, M. R. A. New Method for Experimental Measurement of Diffusion Coefficients in Reservoir Fluids. *J. Pet. Sci. Eng.* **1996**, *14*, 235−250.

(6) Taylor, G. Dispersion of Soluble Matter in Solvent Flowing Slowly Through a Tube. *Proc. R. Soc. London, Ser. A* **1953**, *219*, 186−203.

(7) Cadogan, S. P.; Hallett, J. P.; Maidand, G. C.; Trusler, J. P. M. Diffusion Coefficients of Carbon Dioxide in Brines Measured Using C-13 Pulsed-Field Gradient Nuclear Magnetic Resonance. *J. Chem. Eng. Data* **2015**, *60*, 181−184.

(8) Lu, W. J.; Guo, H. R.; Chou, I. M.; Burruss, R. C.; Li, L. L. Determination of Diffusion Coefficients of Carbon Dioxide in Water Between 268 and 473 K in a High-Pressure Capillary Optical Cell with In situ Raman Spectroscopic Measurements. *Geochim. Cosmochim. Acta* **2013**, *115*, 183−204.

(9) Sell, A.; Fadaei, H.; Kim, M.; Sinton, D. Measurement of CO2 Diffusivity for Carbon Sequestration: A Microfluidic Approach for Reservoir-Specific Analysis. *Environ. Sci. Technol.* **2013**, *47*, 71−78.

(10) Belgodere, C.; Dubessy, J.; Vautrin, D.; Caumon, M. C.; Sterpenich, J.; Pironon, J.; Robert, P.; Randi, A.; Birat, J. P. Experimental Determination of CO2 Diffusion Coefficient in Aqueous Solutions Under Pressure at Room Temperature Via Raman Spectroscopy: Impact of Salinity (NaCl). *J. Raman Spectrosc.* **2015**, *46*, 1025−1032.

(11) Windisch, C. F.; Glezakou, V. A.; Martin, P. F.; McGrail, B. P.; Schaef, H. T. Raman Spectrum of Supercritical (CO2)-O-18 and Re-evaluation of the Fermi Resonance. *Phys. Chem. Chem. Phys.* **2012**, *14*, 2560−2566.

(12) Duan, Z. H.; Sun, R. An Improved Model Calculating CO2 Solubility in Pure Water and Aqueous NaCl Solutions from 273 to 533 K and from 0 to 2000 bar. *Chem. Geol.* **2003**, *193*, 257−271.

(13) Li, X.; Song, Y.; Wu, B.; Liu, Y.; Jiang, L. Determination of Swelling Effect in CO2-Brine Systems Using Microfocus X-ray CT. *Energy Procedia* **2017**, *142*, 3344−3349.

(14) Crank, J. *The Mathematics of Diffusion*; Oxford University Press: Oxford, 1979.

(15) Trebotich, D.; Adams, M. F.; Molins, S.; Steefel, C. I.; Shen, C. P. High-Resolution Simulation of Pore-Scale Reactive Transport Processes Associated with Carbon Sequestration. *Comput. Sci. Eng.* **2014**, *16*, 22−31.

(16) Thomas, W. J.; Adams, M. J. Measurement of Diffusion Coefficients of Carbon Dioxide and Nitrous Oxide in Water and Aqueous Solutions of Glycerol. *Trans. Faraday Soc.* **1965**, *61*, 668−673.

(17) Kestin, J.; Khalifa, H. E.; Correia, R. J. Tables of the Dynamic and Kinematic Viscosity of Aqueous NaCl Solutions in the Temperature Range 20−150-degree-C and the Pressure Range 0.1−35 MPA. *J. Phys. Chem. Ref. Data* **1981**, *10*, 71−87.

DOI: 10.1021/acs.jpcb.8b00802
J. Phys. Chem. B 2018, 122, 4566−4572

(18) Schultz, S. G.; Solomon, A. K. Determination of Effective Hydrodynamic Radii of Small Molecules by Viscometry. *J. Gen. Physiol.* **1961**, *44*, 1189−1199.
(19) Han, P.; Bartels, D. M. Temperature Dependence of Oxygen Diffusion in H2O and D2O. *J. Phys. Chem.* **1996**, *100*, 5597−5602.
(20) Krynicki, K.; Green, C. D.; Sawyer, D. W. Pressure and Temperature-Dependence of Self-Diffusion of Water. *Faraday Discuss. Chem. Soc.* **1978**, *66*, 199−208.
(21) Møller, K. B.; Rey, R.; Masia, M.; Hynes, J. T. On the Coupling between Molecular Diffusion and Solvation Shell Exchange. *J. Chem. Phys.* **2005**, *122*, 114508.
(22) Hynes, J. T.; Kapral, R.; Weinberg, M. Molecular Theory of Translational Diffusion − Microscopic Generalization of the Normal Velocity Boundary-Condition. *J. Chem. Phys.* **1979**, *70*, 1456−1466.
(23) Price, W. S. Pulsed-Field Gradient Nuclear Magnetic Resonance as a Tool for Studying Translational Diffusion 0.1. Basic Theory. *Concepts Magn. Reson.* **1997**, *9*, 299−336.
(24) Momot, K. I.; Kuchel, P. W. PFG NMR Diffusion Experiments for Complex Systems. *Concepts Magn. Reson., Part A* **2006**, *28A*, 249−269.
(25) Knoche, W. In *Chemical Reactions of CO_2 in Water: Biophysics and Physiology of Carbon Dioxide*; Bauer, C., Gros, G., Bartels, H., Eds.; Springer: Heidelberg, 1980; pp 3−11.

DOI: 10.1021/acs.jpcb.8b00802
J. Phys. Chem. B 2018, 122, 4566−4572